Indoor Solar Energy Harvesting for Sensor Network Router Nodes

Abhiman Hande[*]*, Todd Polk, William Walker, and Dinesh Bhatia*[*]

Erik Jonsson School of Engineering and Computer Science, University of Texas at Dallas, P.O. Box 830688, EC33, Richardson, TX 75083

* Authors to whom correspondence should be addressed.
Emails: Abhiman Hande (abhiman.hande@utdallas.edu), Dinesh Bhatia (dinesh@utdallas.edu).

Abstract

A unique method has been developed to scavenge solar energy from monocrystalline solar cells to power wireless router nodes that are used in indoor applications. This method eliminates the need to use alkaline batteries that require frequent replacement from time to time. The system consists of two key components viz. an energy harvesting unit and an energy storage module. The energy harvesting module consists of an adequate number of solar cells connected in series-parallel combination to scavenge energy from overhead 34 W fluorescent lights that are always operational in office and hospital hallways. A set of ultracapacitors were used as the energy storage device and alkaline batteries were used only as a back-up energy source. The router nodes (Crossbow MICAz motes) controlled the operation of the energy scavenging circuit in order to harvest adequate amounts of energy for optimal performance. In order to minimize power consumption, two router nodes (each with 50 % duty cycle) were used as a router pair so that at any point in time only one router node was in the on state while the other was in a sleep state drawing negligible power. The system set-up was tested using one sensor node that routed data at a fairly high frequency of 0.1 Hz through a router pair to the base-station. Test results show that the harvesting circuit which acted as a plug-in to the MICAz router nodes manages energy harvesting and storage, and enables near-perpetual, harvesting aware operation of the router node.

1. Introduction

The application spectrum of wireless sensor and actuator networks seems to be growing without bounds. Some of the applications include temperature and light monitoring in remote locations, sensing chemicals in traffic congested areas, and measuring tire pressure and monitoring acceleration in automobiles. Each wireless node is intended to be deployed to a remote location to sense critical data and relay its measurements to other network nodes for monitoring and control purposes. Many foresee these embedded system devices in applications ranging from industrial automation to home networking [1,2]. These smart networks represent the next evolutionary development step in building, utilities, industrial, home, shipboard, and transportation systems automation.

Wireless sensor networks (WSNs) focused towards indoor industrial and biomedical applications face serious challenges in terms of harvesting nearby natural sources of energy for power. Presently, such network nodes use alkaline batteries as sources of energy. Obviously, these batteries have a fixed energy rating and therefore, a limited life. They have to be replaced in due time and this factor plays a major role in determining the life of a wireless sensor node. For example, a Crossbow MICAz mote [3] operating at 1% duty cycle on standard 3000 milli-ampere-hour (mAhr) AA batteries would require battery replacement every 17.35 months [4]. Often, the cost of physically deploying resources to change a node's worn out battery outweighs the cost of the node itself. The issue of powering these nodes becomes critical when one considers the prohibitive cost of wiring power to them or replacing their batteries. To make matters worse, battery technology hasn't improved in terms of energy density and size over the last decade, especially for low power applications such as sensor networks [5]. While an effort is being made to improve the energy density of batteries, additional energy resources need to be investigated to increase the life of sensor network nodes. Exploiting renewable energy resources in the device's environment, offers a power source limited by the device's physical survival rather than an adjunct energy source.

It is therefore necessary to exploit energy sources ubiquitous to a sensor node's operating space in order to obtain the possibility of infinite lifetime. It is possible to scavenge energy from several sources, and there has been a concerted effort towards a detailed comparison of energy per unit area available, and cost of the corresponding scavenging schemes [6,7]. Some of the available harvesting technologies include solar cells, piezoelectric vibration generators, and energy from thermal and acoustic noise. Table 1 compares the power generation potential of some of these energy harvesting modalities. Among these sources of energy, solar energy harvesting through photovoltaic conversion and vibrational energy through piezoelectric elements provide relatively higher power densities. This makes them the modalities of choice to power a WSN that consumes power on the order of several mW. However, the design of an efficient energy harvesting module involves complex tradeoffs due to the interaction of several factors such as the characteristics of the energy sources, chemistry and capacity of the energy storage device(s) used, power supply requirements, and power management features of the embedded system, and application behavior. It is therefore essential to thoroughly understand and judiciously exploit these factors in order to maximize the energy efficiency of the harvesting

modules. Moreover, the power output from these natural sources is highly nonlinear in nature and depends upon a variety of factors.

From Table 1, it is clear that solar energy is the most efficient natural energy source available for sensor networks used for outdoor applications. However, for indoor applications, it is important to note that the efficiency of photovoltaic cells is very low. Typically, the light intensity under artificial lighting conditions found in hospitals and offices is less than 10 W/m^2 as compared to 100-1000 W/m^2 under outdoor conditions. For example, monocrystalline solar cells have an efficiency of less than 1-3% under typical indoor lighting conditions [8]. In spite of such poor efficiencies, these cells still have a power density of at least 0.5-1 mW/cm^2 under indoor 1-5 W/m^2 light intensity conditions, which is much higher than their nearest energy scavenging competitor. Although amorphous solar cells have been found to have slightly higher efficiencies of 3-7% under indoor conditions [8], they are much more expensive than their monocrystalline counterparts. This paper therefore focuses on scavenging energy from monocrystalline photovoltaic cells.

2. WSNs in Indoor Applications

There are several indoor applications that seem feasible for WSNs. But to eliminate their dependence on batteries and use solar cells as an exclusive energy source would require the indoor lights to be on continuously and would therefore, seem to be impractical for a variety of indoor applications. However, indoor WSNs operating on solar power appear to be feasible for industrial and hospital environments where indoor lights are operational at a duty cycle close to 100%.

Figure 1 shows one such concept of an in-hospital WSN that can be used to monitor patient vital sign data from instruments such as electrocardiograms (ECGs) [9], pulse oximeters [10], and blood pressure (BP) monitors [11]. These units can be interfaced to WSN nodes that are programmed as sensor nodes. These sensor nodes are required to perform the function of sensing vital sign data from the patient and are typically required to be ambulatory in nature. Therefore, it is more convenient to allow them to run on stable sources of energy such as batteries. The maximum range of data transmission for such nodes is approximately ten meters [4]. Thus, additional nodes may be required to pass the data back to the central monitoring location. There might be several such router nodes distributed in these WSNs, and their density and number

would depend on the hospital size and coverage requirements. Typically, each router node in the network has a fixed location and its only function involves establishing itself in the network and enabling prompt data transfer to the nearest router node or base-station. These router nodes obviously need to be continuously on so that data can be promptly transferred. Since hospitals have fluorescent lights in the hallways that are always on, it is advantageous to operate these router nodes by scavenging light energy. This would result in a huge cost savings over time (this arrangement eliminates the need to monitor and replace batteries). Referring to figure 1, the base-station in such networks consists of a mote that receives data and is connected to a server. The data received by the base-station is displayed to allow constant patient monitoring and can be routed to the patient's physician for easy access in real-time. Similarly, WSN router nodes in industrial plants and corporate offices can scavenge energy through overhead fluorescent lights rather than use batteries. In fact, in such systems, sensor nodes might not be mobile and therefore, it might be possible and advantageous to power the sensor nodes (in addition to router nodes) through photovoltaic solar cells.

3. Energy Harvesting Methodology

A simplified block diagram of a wireless router node operating on solar energy is shown in Figure 2. Typically, a router node consists of an eight-bit microcontroller with adequate resources to operate its kernel [12]. The microcontroller manages power to the sensors and data acquisition elements, as well as responds to commands from the base-station. Crossbow MICAz motes were used as the router nodes of the system. Each MICAz mote uses the Chipcon CC2420, IEEE 802.15.4 compliant, Zigbee ready radio frequency transceiver [13] integrated with an eight-bit ATMega 128L microcontroller [14]. The system communicates in the 2.4GHz frequency band.

Several key issues were addressed before embarking upon designing the indoor solar energy scavenging prototype circuit. Firstly, solar energy has to be harvested by an efficient energy scavenging system, and secondly, there has to be an efficient means of storing this harvested energy [15]. The system must also effectively deliver the stored energy to the router node. This means there has to be an intelligent power management strategy in place. Obviously, this strategy must not be power hungry and should serve to lengthen the life of the energy storage devices. These details along with design considerations that impact efficiency and the associated

tradeoffs are explained in the next few sections.

3.1 Solar Cell Characteristics

Solar cells have vastly differing characteristics from batteries. As mentioned in section 1, there are several kinds of photovoltaic cells available and all of them are relatively inefficient under indoor light conditions [8]. Since amorphous cells are much more expensive than their monocrystalline counterparts, it was decided to use monocrystalline cells as the source of natural energy.

3.75" x 2.5", 4-4.0-100 monocrystalline solar panels from Solar World Inc. [16] were chosen for the system due to ease of availability and low cost. Each panel was rated at 100 mA short circuit current (I_{SC}) and 4 V_{DC} open circuit voltage (V_{OC}) under 1 sun (1000 W/m^2) conditions. In order to determine the number of panels required per router node, a simple load test was conducted. A single 4-4.0-100 Solar World panel was connected across a varying load to determine its V-I profile. The panel was placed at a 1 cm distance from overhead 34 W Phillips fluorescent F34CW/RS/EW lights. These lights are representative of those used in indoor office and hospital environments. Figure 3 shows the V-I profile wherein it can be observed that at around 3.2 V_{DC} the panel sourced out approximately 2 mA. A Crossbow MICAz node when active will draw a minimum of 25 mA under full load condition at 3 V_{DC} [4]. Therefore, at least twelve panels were required per router node. Although the size of the panels was not a concern, a modularized approach (described in the following section) was taken in order to reduce the panel size further. It was decided to use two router nodes with 50% duty cycle as a router pair rather than using a single router node that is always on. This would obviously add some cost to the system due to the addition of an extra router node per router pair, however, it reduces the size of each router node's solar panel configuration. In addition, low power Maxwell PC5-5, 5 V_{DC}, 2F ultracapacitors [17] were used in parallel with the solar panels to store the harvested energy and to reduce the solar panel power rating requirement even further. These details are explained in the next few sections.

3.2 Network Protocol

A multi-hop mesh network was designed for the system. The network architecture consists of several router pairs that provide paths for sensor nodes to send data to or receive data from the

base-station. This strategy helped minimize the size of solar panels required by each router node. Figure 4 shows the conceptual diagram of the network. The figure shows four router pairs each comprised of their own router nodes R_1 and R_2. A special dual router (DR) algorithm was used to control the operation of R_1 and R_2. Here, at any point in time either R_1 or R_2 would be on but not both. This indicates a 50% duty cycle for both R_1 and R_2 at every router pair and therefore, a reduced solar panel size per router node. In figure 4, sensor nodes S_1, S_2, and S_3 use router pairs 1 and 2, and sensor nodes S_4, S_5, and S_6 use router pairs 3 and 4 to transmit their sensor measurements to the base-station.

Figure 5 shows the flowchart for both R_1 and R_2. At start-up, several key parameters of the router node are initialized to appropriate values before commencing the DR algorithm. This includes initialization of the router node microcontroller and transceiver. After the initialization process is completed, the router node tries to find an established network. It continues transmitting connection requests until it receives a response from at least one other node. It will then choose a node that is closest to the base-station (i.e., shortest path or minimum hop count). The base-station comprises of another MICAz mote and could be either one hop away from the new router node or multiple hops away. The new node will then request a network ID. This request is forwarded to the base-station, which responds to the router node's request and assigns it a network ID. The newly ID'ed router node next checks for its nearest route partner. For example, referring to figure 4, in every router pair, after R_1 and R_2 receive their respective IDs from the base-station, they try locating and finding each other, leading to eventual collaboration and the formation of a router pair. The router pair is then fully functioning and begins its operation at 50% duty cycle. Figure 4 indicates four such router pairs each with their own respective R_1 and R_2 router nodes. If for some reason a router node is unable to communicate with its partner, it will first attempt to reconnect to that partner node. If it is unsuccessful, it will attempt to find a new partner.

After locating its corresponding partner, each router node and its partner use a DR algorithm to facilitate a 50% duty cycle. Initially, R_1 forces R_2 to enter a sleep mode. Here, R_2's microcontroller and transceiver are forced into a low power mode in order to minimize power consumption (on the order of tens of μW). An asynchronous timer is used to set the sleep time. After the prescribed sleep interval is completed, the timer generates an interrupt that causes R_2 to wake up. The wake up routine transmits a sleep packet to R_1 ordering it to enter a similar sleep

state. Now, R_1 enters its sleep mode and R_2 remains awake. After R_1's sleep interval is completed, its asynchronous timer generates an interrupt causing it to wake up and send a sleep packet to R_2 forcing it to sleep again. This on-off cycle continues for R_1 and R_2 at every router pair so that at any point in time either R_1 or R_2 is always available to route a potential packet emanating from a sensor node towards the base-station or vice-versa. The DR algorithm for R_1 and R_2, therefore, sits in an infinite loop collaborating with its route partner to execute a 50% duty cycle. Therefore, any one router node in a router pair is always awake and is ready to route a packet from a router pair at a higher hop count (or its own affiliated sensor node) towards the base-station via other router pairs that have a lower hop count or vice-versa. The on-off time period for R_1 and R_2 does depend on the energy storage and scavenging mechanism.

Figure 6 shows the flowchart of a typical sensor node in the network. The initial start-up routine is fairly similar to the router nodes. A sensor node affiliates itself with the closest router pair to the base-station. For example, figure 4 shows three sensor nodes viz. S_1, S_2, and S_3 that are associated with router pair 2. Here, sensor readings from any of these sensor nodes are transferred to the base-station via router pairs 1 and 2. Similarly, sensor nodes viz. S_4, S_5, and S_6 use router pairs 3 and 4 to communicate with the base-station. Depending upon the application, sensor readings are transmitted at prescribed intervals. After transmitting the packet, the sensor node enters a low power sleep state to minimize power consumption. Once again, the microcontroller's asynchronous timer is used to execute the sleep operation. Obviously, since the sensor nodes used in indoor networks (such as the example described in section 2) will not have a fixed location, it is impractical to implement a solar energy harvesting system for these nodes. However, other schemes such as piezoelectric vibration generators and thermal energy scavenging systems can possibly be used for energy harvesting purposes. These schemes will be explored in our future work. In the present system, alkaline batteries were used to power the sensor nodes.

4. Power Management

An energy harvesting scheme similar to figure 7 was used for the router nodes. It consists of an adequate number of solar panels to charge the energy storage devices which in turn output regulated power to the router node. More often than not, this strategy works well for outdoor environments where adequate solar energy is available during the day to charge the energy

storage devices. However, as described in sections 2 and 3, in many indoor applications, solar energy scavenging from overhead 34 W fluorescent lights is fairly practical. This strategy was utilized to obtain power for the router nodes. From figure 7, the core of the energy harvesting module is the power management circuit, which draws power from the solar panels and manages energy storage and power routing to the router node. The most important consideration in the design of this circuit is to maximize energy efficiency, enhance device reliability, and lengthen the life of the router node. The power management circuit designed for this system provides regulated power to the router node and also simultaneously stores energy in ultracapacitors.

Figure 8 shows the simplified schematic of the actual energy harvesting circuit with alkaline batteries used as back-up power. An adequate number of solar panels (S) were used to support charging of the ultracapacitor bank (C). Initial tests were conducted wherein a power supply was used to simulate the solar panel bank to determine the number of panels required. The ultracapacitor bank comprised of two Maxwell PC5-5 ultracapacitors. As mentioned in section 3, solar panels have an optimal operating point that provides maximum power output. The ultracapacitors ensure operation at about this power point by clamping the output terminals of the solar panel to approximately 3 V_{DC}. During normal router node operation, energy from both the ultracapacitor and solar panel bank is used. When the router node is on, energy is drawn from both power sources almost equally and when the node enters its sleep state, it draws minimum power from both sources. During the sleep state, the solar panel bank charges the ultracapacitors back to about 3 V_{DC}. The voltage ripple due to capacitor charge and discharge during the on-off cycles was found to be minimal and therefore, was not a cause of concern. A 3.6 V_{DC} zener clamping diode was used to protect the router node from excessively high voltages.

Two p-channel MOSFETS (Q_1 and Q_2) were used as switches to allow the use of alkaline batteries for emergency back-up power. PC_0 and PC_3 (Port C of the microcontroller) were used to control the operation of Q_1 and Q_2 respectively. During normal router node operation, PC_0 = '0' and PC_3 = '1' so that Q_1 is on and Q_2 is off. This facilitates router node operation by drawing power from the solar panels and ultracapacitor bank. During adverse conditions when energy is not available from the solar panel bank, PC_0 = '1' and PC_3 = '0' so that Q_1 is off and Q_2 is on. Now, energy from the back-up battery is used to power the router node. ADC_3 (Port F of the microcontroller) was used to continuously monitor the ultracapacitor voltage and obtain a voltage reference for the router node microcontroller. Due to possible variation in supply voltage

(V_L), a fixed 1.223 V_{DC} voltage reference was used to determine the router node V_L and microcontroller 10-bit A/D reference voltage (V_{REF}). This voltage reference consisted of a 1.223 V_{DC} zener diode that was part of the microcontroller IC. ADC_7 (Port F of the microcontroller) was used to measure this fixed 1.223 V_{DC} voltage reference. For example, if 'D_1' corresponds to the digitized 1.223 V_{DC} input ADC_7 value,

$$V_L = V_{REF} = (1.223 \times 1024) / D_1 \qquad (1).$$

The calculated V_{REF} was in turn used to determine the ultracapacitor voltage (V_C) in the router node software. If D_2 corresponds to the digitized ADC_3 value,

$$V_C = (D_2 \times V_{REF}) / 1024 \qquad (2).$$

The safe operating range of the router node microcontroller, transceiver, and peripheral circuitry is in the 2.7 to 3.6 V_{DC} range. Therefore, a simple back-up power supply algorithm was inserted in the router node software which operated as indicated below:

1. Under normal operation, PC_0 = '0' and PC_3 = '1'. Therefore, Q_1 is on and Q_2 is off, and energy is routed from the solar panel-ultracapacitor bank to the router node.

2. If solar energy is lost (for example, a fluorescent light turns off or fails), then the ultracapacitor charge will begin to drop resulting in a gradual reduction in supply voltage until $ADC_3 < 2.7$ V_{DC}. At this point, PC_0 = '1' and PC_3 = '0'. Therefore, Q_1 is off and Q_2 is on, and energy is routed from the back-up 3 V_{DC} alkaline battery (V_B) to the router node. In such a situation, the measured ADC_3 value ('D_1') is transmitted to the base-station to indicate a potential problem in the solar panel-ultracapacitor bank.

3. If the router node is drawing power from V_B and the solar energy source is restored, the router node waits for its ultracapacitor to be charged to 3.4 V_{DC}, and then switches back to solar power, i.e., PC_0 = '0' and PC_3 = '1'. During this condition, V_C is greater than V_B (= V_{REF}), and therefore a simple resistor divider circuit was used for voltage scaling purposes in order to scale V_C down below 3 V_{DC} and facilitate correct V_C measurements.

5. Experimental Results

In order to determine the right number of solar panels for powering each router node a simple load simulation test was first conducted. Figure 9 shows a power supply simulating the source solar panel and a load resistance simulating the router node load. A signal generator was used that supplied a 5 V_{DC}, 0.5 Hz, 50% duty cycle square wave signal (V_{SG}) to the base of a BJT connected between the power source and the load resistance. The intention was to simulate a router node turning on and off every second at 50% duty cycle.

Figure 10 shows the steady state waveforms obtained during these tests. As can be seen from figure 10, when the load is on and draws power from the source, current is supplied from both the power supply as well as the ultracapacitor bank. For example, in the 1-2 second interval, initially the current supplied from the power supply (I_P) equaled 11.3 mA and the current obtained from the ultracapacitor bank (I_C) equaled 9.7 mA. At about 2 seconds, a higher I_P current equal to 11.8 mA was required and a lower current of 9.2 mA is delivered by the ultracapacitors. This is because under load conditions, the capacitor voltage drops slightly resulting in a lower I_C and higher I_P requirement. However, in both instances the total current from the power supply-ultracapacitor bank equaled about 21 mA. During the off intervals the power supply charges the ultracapacitors. Referring to the 2-3 second interval in figure 10, I_C has a negative initial value of about 9.7 mA at 2 seconds. In this phase, the lost capacitor charge during the previous load condition is replenished by the power supply. As the capacitors charge, their terminal voltage builds up resulting in a lower current requirement of about 9.2 mA from the power supply at 3 seconds. The load voltage (V_L) during the on-off operation cycles stabilized at about 3.24 V_{DC} under steady state conditions. The maximum current drawn from the power supply when the router node turned on equaled approximately 12 mA. This implies that around six solar panels would be required to generate a similar amount of current. However, in a later test, when the power management circuit was inserted, it was found that the current requirement increased to approximately 14 mA. This indicated a solar panel requirement of at least seven panels. As a factor of safety, it was decided to use eight solar panels in series-parallel to satisfy the power requirements for the energy scavenging circuit.

Next, the energy harvesting circuit was built on a protoboard. Figure 11 shows a Crossbow MICAz router node with its corresponding energy harvesting circuit board and back-up battery power supply. The size of each router node was fairly compact at 2.5” x 2.25” x 1”. An

experiment was conducted to measure the overall efficiency of the energy harvesting circuit at a load current of about 25 mA at 3 V_{DC}. For this experiment, a power supply was used as the energy source instead of the solar panel, and a potentiometer was used as the load to set the load current to the prescribed value. V_L and V_C were found to differ by only about 60 mV at a load current of 25 mA. The power supply current (I_P) was found to be about 30 mA during this test and therefore, the overall circuit efficiency was determined as follows:

$$\eta = ((V_L \times I_L) / (V_C \times I_C)) \times 100 = ((3 \times 25) / (3.06 \times 30)) \times 100 \cong 82\% \qquad (3).$$

After obtaining satisfactory results in the above tests, two MICAz motes were programmed as a router pair (R_1 and R_2) and one mote was programmed as the base-station. The base-station mote was connected to a PC via its serial port. Figure 12 shows the router node voltage (V_L) and the ultracapacitor voltage (V_C) waveforms for R_1. A one second on-off time was found to work well. In figure 12, the oscilloscope channel 2 waveform represents V_L and channel 3 represents V_C. It can be observed that both waveforms overlap each other indicating minimal voltage drop across Q_1 and V_C stabilized at about 3.06 V_{DC} during the test. During the sleep (off) interval, R_1 offers extremely high impedance to the solar panel-ultracapacitor bank resulting in a current consumption on the order of tens of μA. From figure 8, since the $R_{DS(ON)}$ of Q_1 is very low, almost all of V_C is dropped across V_L during the sleep interval. Since much higher current flows through Q_1 during the on interval, not all of V_C is available at the load end. In fact, from figure 13 at a much lower 100 mV/division scale, it can be observed that about 50 mV was found to account for Q_1's $R_{DS(ON)}$ during this on phase. Since Q_1's $R_{DS(ON)}$ was approximately 2 Ω at 25 mA drain current, a 50 mV voltage drop across its drain and source seemed about right. Figure 13 also shows the ultracapacitor charge and discharge cycles during R_1 off and on phases respectively. Also, during the R_1 off state, V_L and V_C can be seen to differ by about 10 mV which is possibly due to the leakage through the zener diode and other circuit components. The voltage ripple for V_C was minimal and equaled about 15 mV indicating a very low ripple factor of about 0.49%. Figure 14 shows a snapshot of V_L and V_C for both R_1 and R_2. Here, oscilloscope channels 2 and 3 were used for R_1, and channels 1 and 4 were used for R_2 to represent V_L and V_C respectively. It can be observed that each router node has a one second on-off interval. Moreover, when R_1 is on, R_2 is asleep, and vice-versa so that R_1 and R_2 are never on at the same time. Just as in figure 12, V_C for both router nodes stabilized at about 3.06 V_{DC}.

In another test, the preliminary application framework was tested with one sensor node and two router nodes that acted as a router pair. All three nodes were programmed to route their supply voltage (V_L) to the base-station intermittently. The sensor node V_L data was used to simulate a sensor reading. The intention was to first comprehensively test the network framework and solar energy scavenging system before attempting to use the system in an industrial or hospital environment. The router nodes also transmitted their V_L intermittently to enable the base-station to monitor and detect a possible failure in the solar panel-ultracapacitor bank. Each router node was powered through photovoltaic solar cells that scavenged energy from 34 W fluorescent lights. Figure 15 shows the set-up of a router node's corresponding solar panels located close to the overhead lights. Both the router nodes operated at 50% duty cycle so that at any point of time one of them is on while the other is asleep. Data received by the base-station mote was first stored in its on-chip memory and then transferred to the PC for analysis. A simple terminal program was designed in order to monitor incoming data from the base-station in real-time using the PC RS232 port. A test was conducted wherein the sensor and router nodes were left operational for more than a day. This test was necessary to observe the robustness of the system. Figure 16 shows a snapshot of the terminal program after 24 hours of operation, where the sensor node (S_1) relays its V_L approximately every ten seconds to the base-station. A relatively high 0.1 Hz data transmission frequency was chosen for this experiment. Referring to figure 16, nodes 1 and 2 are numbered as the two router nodes (R_1 and R_2) respectively, and the sensor node S_1 is identified as node 3. In this experiment, only one router pair was used to transfer data from S_1 to the base-station. The information received at the base node is in the format shown in Figure 17. It can be observed that node 3 (S_1) used router node 2 (R_2) to route its V_L (which equaled $CE6_{16}$, i.e., 3302 mV) to the base-station at 13:05:11. The next set of data sent from node 3 is received at the base-station ten seconds later at 13:05:21. Also, in addition to the sensor node, both router nodes transmit their V_L to the base-station approximately every thirty seconds. From, figure 16 it can be observed that 13:05:45, node 1 (R_1) had a V_L equal to $B8B_{16}$, i.e., 2955 mV and at 13:05:49, node 2 (R_2) had a V_L equal to $BC5_{16}$, i.e., 3013 mV. This verifies that the voltage obtained from each router node's solar panel-ultracapacitor bank stabilized at an optimum load voltage of about 3 V_{DC}. Similar results were obtained when the system framework was later tested with two router pairs to route the sensor node battery voltage to the base-station.

6. Conclusions

The technique of scavenging solar energy for WSN router nodes that are used in indoor applications proved to be very effective. The method used for energy scavenging is quite straightforward and is not restricted to one particular type of indoor application. Several tests were carried out in order to evaluate the energy scavenging scheme. The 50% duty cycle per router node and the use of ultracapacitors to aid the solar panel bank resulted in a reduced solar panel power requirement. This strategy lowered the power rating of the energy scavenging circuit and therefore, reduced the circuit size and cost. Also, this accounted for a lesser number of solar panels per router node resulting in a modularized and compact design. The energy harvesting and power management circuit was found to be fairly efficient at about 82% which indicates minimal energy wastage. The preliminary network protocol was found to be fairly robust and the steady state V_L requirement from each router node's energy scavenging circuit stabilized at about 3 V_{DC} which turns out to be the optimum power supply voltage for the node's microcontroller and transceiver.

The router node size will be reduced even further by implementing the energy harvesting and power management circuit on a printed circuit board. The future project directions involve identifying valid indoor applications for such a system. One such example involves a remote healthcare monitoring system wherein vital sign sensors such as ECG, BP monitors, and pulse oximeters are interfaced to sensor nodes and their measurements are routed to a base-station. In hospital settings, such systems will fair extremely well to monitor patient activity without needing the patient to be confined to his bed. Another interesting application involves design of remote at-home healthcare monitoring systems which monitor patient vital sign data. Here, a sensor node routes data to a base-station that has internet access and is located within the household premises. This base-station in turn transfers incoming data to a website database in a secure fashion, and therefore enables the doctor to monitor the patient's health from a remote location in real-time. Such systems however, need to be reconfigurable so that a doctor has the resources to interface a variety of vital sign sensors to a sensor node and download its corresponding software before handing the sensor node to a patient. To this effect, an effort is underway to interface an A&D Medical UA767PC BP monitor [18] to MICAz sensor nodes in order to facilitate remote monitoring of systolic and diastolic blood pressure, and heart-rate data [19].

7. Acknowledgements

This research was conducted in the Embedded and Adaptive computing group at the University of Texas at Dallas (UTD), and the work was carried out in the ambient computing and sensor network (ACSN) laboratory. The authors would like to acknowledge the advice and assistance provided by Dr. Padmakar Kulkarni from University of Texas Southwestern Medical Center.

8. References

[1] J. Rabaey, M. Ammer, J. da Silva, D. Patel, and S. Roundy, "PicoRadio Supports Ad Hoc Ultra-Low Power Wireless Networking", IEEE Computer, Vol.33, Issue.7, pp.42-48, July 2000.

[2] B. Gates, "The Disappearing Computer", The Economist, Special Issue: The World in 2003, pp.99, December 2002.

[3] Crossbow Technology Inc., "MICAz Developer's Kit", 2005, http://www.xbow.com/Products/productsdetails.aspx?sid=105.

[4] Crossbow Technology Inc., "MPR/MIB User's Manual, Rev. B, Document 7430-0021-06", 2005, http://www.xbow.com/Support/Support_pdf_files/MPR-MIB_Series_Users_Manual.pdf.

[5] J. Paradiso and T. Starner, "Energy Scavenging for Mobile and Wireless Electronics", IEEE Pervasive Computing, Vol. 4, Issue 1, pp. 18-27, January-March, 2005.

[6] S. Roundy, P. Wright, and J. Rabaey, "Energy Scavenging for Wireless Sensor Networks with Special Focus on Vibrations", ISBN 1-4020-7663-0, Kluwer Academic Publishers, 2004.

[7] V. Raghunathan, A. Kansal, J. Hsu, J. Friedman, and M. Srivastava, "Design Considerations for Solar Energy Harvesting Wireless Embedded Systems", Fourth International Symposium on Information Processing in Sensor Networks Proceedings, pp.457-462, April 2005.

[8] J.F. Randall and J. Jacot, "The Performance and Modelling of 8 Photovoltaic Materials under Variable Light Intensity and Spectra", World Renewable Energy Conference VII Proceedings, Cologne, Germany, 2002.

[9] HealthFrontier Inc., "ecgAnywhere", 2005, http://www.healthfrontier.com.

[10] Smiths Medical PM, Inc., "BCI Micro Power Oximeter Board", 2005, http://www.smiths-bci.com/html/Products/oem_products.htm.

[11] A & D Medical, Inc., "UA-767BT Wireless Blood Pressure Monitor", 2005, http://www.lifesourceonline.com/products/telemonitoring.cfm.

[12] S. Arms, C. Townsend, D. Churchill, J. Galbreath, and S. Mundell, "Power Management for Energy Harvesting Wireless Sensors", SPIE International Symposium on Smart

Structures and Smart Materials Proceedings, March 2005.

[13] Chipcon Technologies, "Chipcon CC2420 2.4 GHz IEEE 802.15.4/Zigbee-ready RF Transceiver", 2004, http://www.chipcon.com/files/CC2420_Data_Sheet_1_2.pdf.

[14] Atmel Inc., "ATMega 128L Microcontroller Datasheet", 2004, http://www.atmel.com/dyn/resources/prod_documents/doc2467.pdf.

[15] M. Rahimi, H. Shah, G. Sukhatme, J. Heideman, and D. Estrin, "Studying the Feasibility of Energy Scavenging in a Mobile Sensor Network", IEEE International Conference on Robotics and Automation Proceedings, pp. 19-24, 2003.

[16] Solar World Inc, "3.75" x 2.5", 4-4.0-100 monocrystaline solar panels", 2005, http://www.solar-world.com/.

[17] Maxwell Technologies, "PC5-5 Ultracapacitor Product Information", 2005, http://www.maxwell.com/ultracapacitors/products/PC5-5.html.

[18] A & D Medical, Inc., "UA-767PC Wireless Blood Pressure Monitor", 2005, http://www.andmedical.com/and_med.nsf/html/UA-767PC.

[19] W. Walker, T. Polk, A. Hande, and D. Bhatia, "Remote Blood Pressure Monitoring using a Wireless Sensor Network", under review, Sixth Annual Emerging Information Technology Conference, Dallas, Texas, August 2006.

List of Figures and Tables

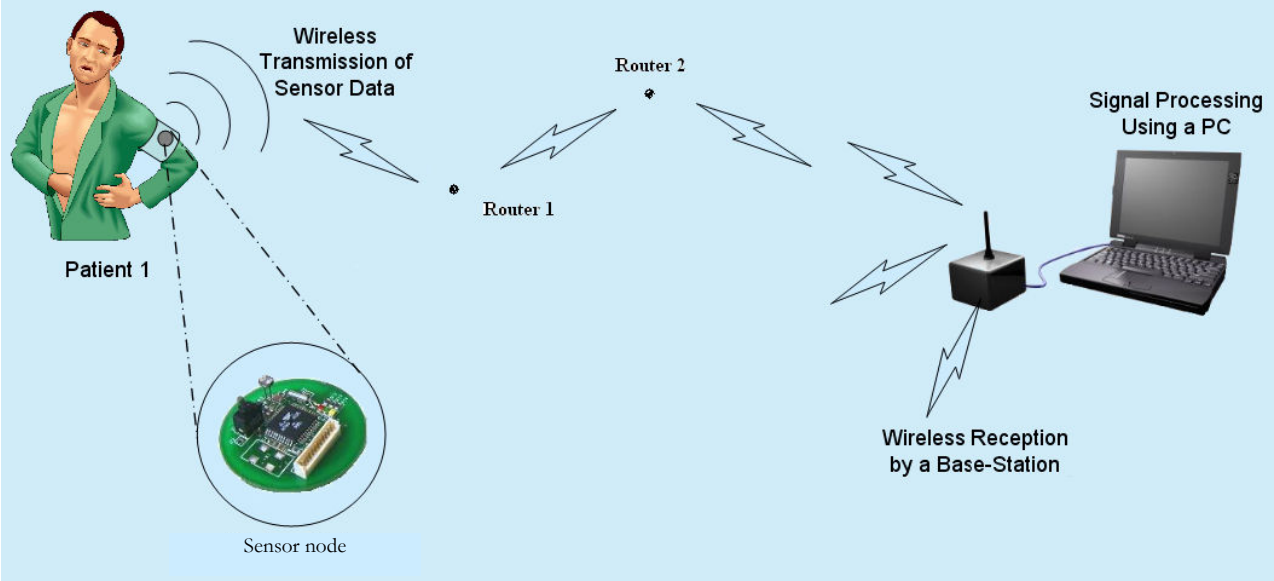

Figure 1. Patient remote health monitoring.
(Figure source:
http://www.enel.ucalgary.ca/People/Haslett/WCLM/CCHE/WebPage/VijayDevabhaktuni_Wireless_Proceedings.doc)

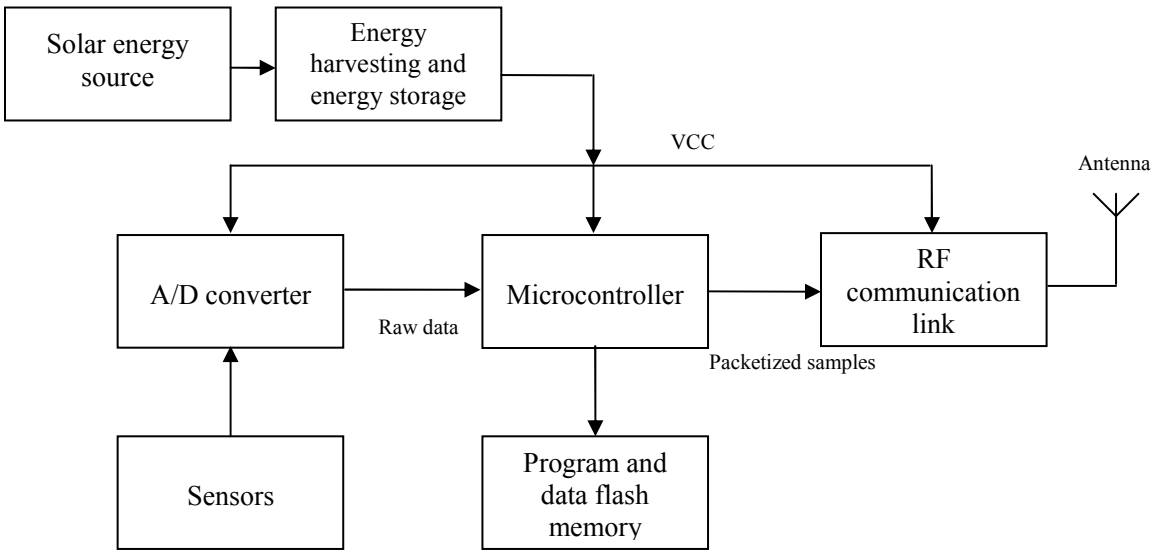

Figure 2. Block diagram of a solar energy harvesting wireless router node.

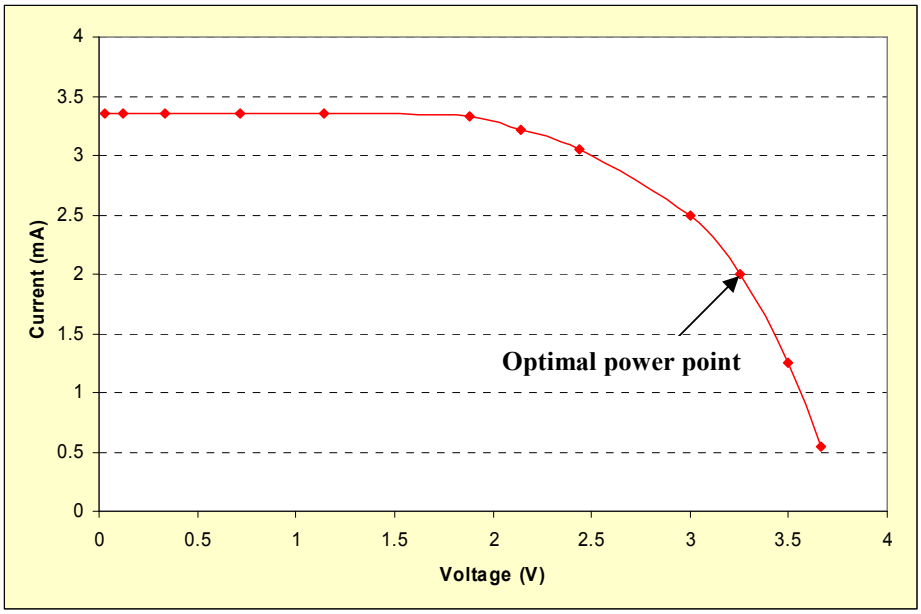

Figure 3. V-I characteristics of a Solar World 4-4.0-100 solar panel under indoor lighting conditions.

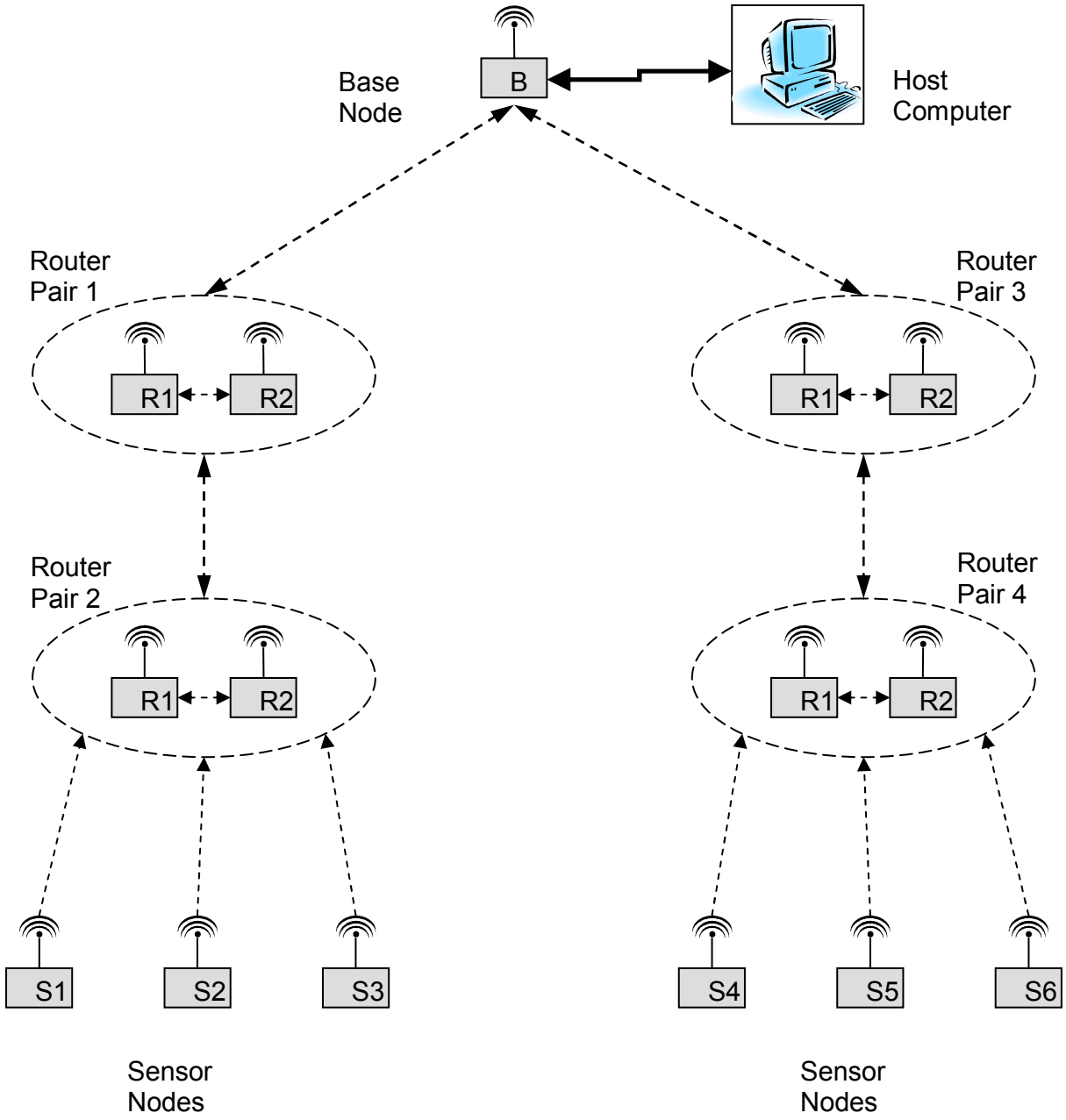

Figure 4. Network structure.

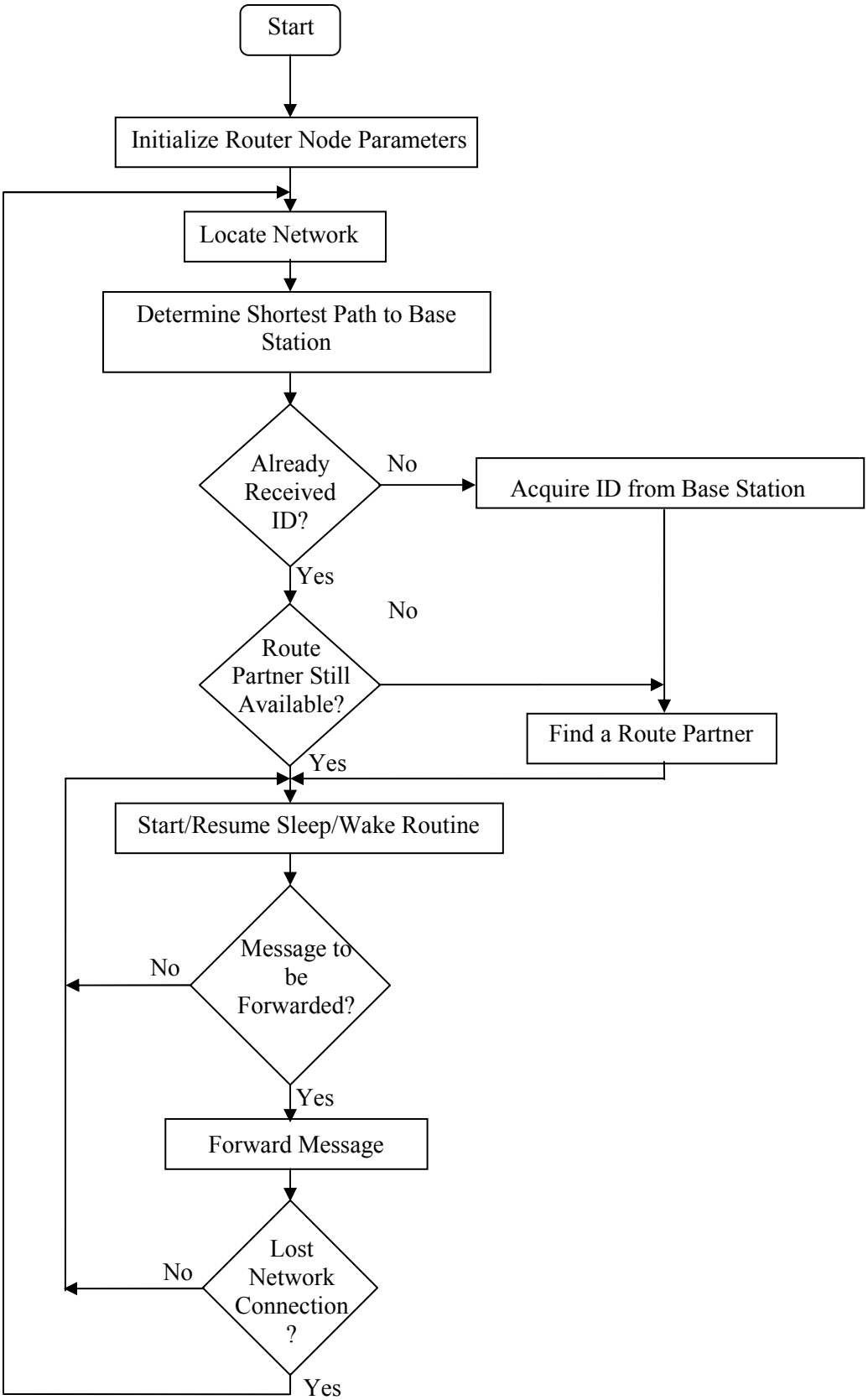

Figure 5. Router node flowchart.

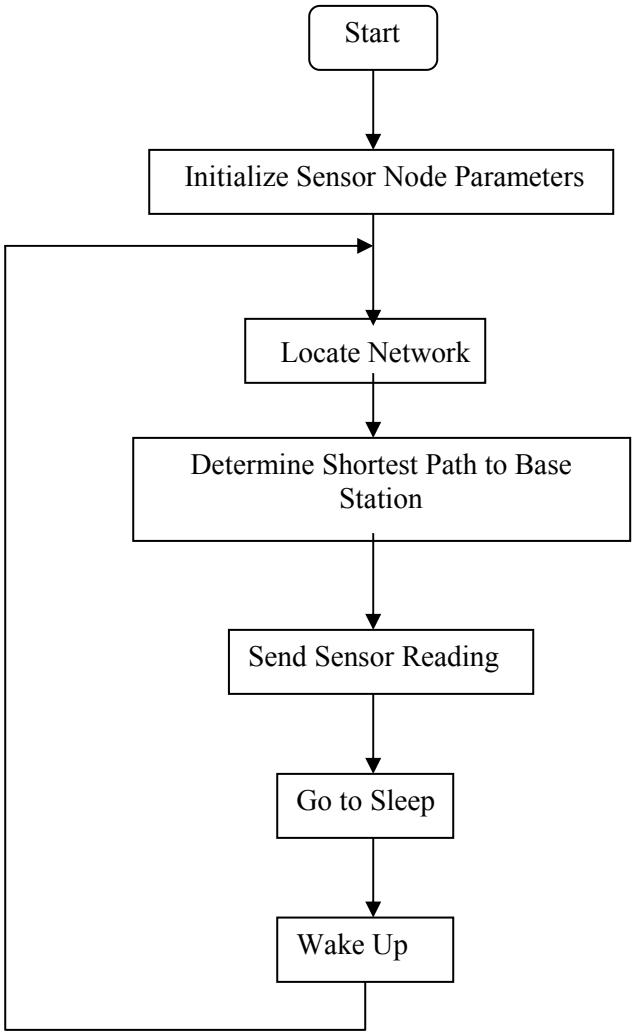

Figure 6. Sensor node flowchart.

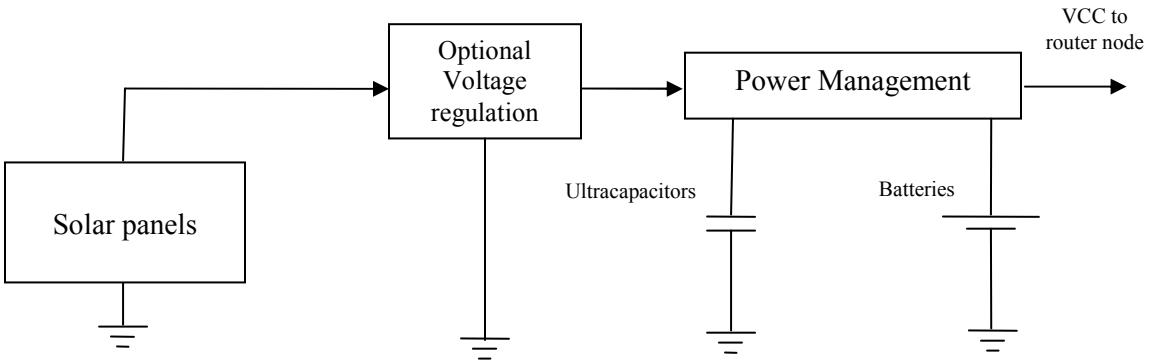

Figure 7. Block diagram of a solar energy harvesting system.

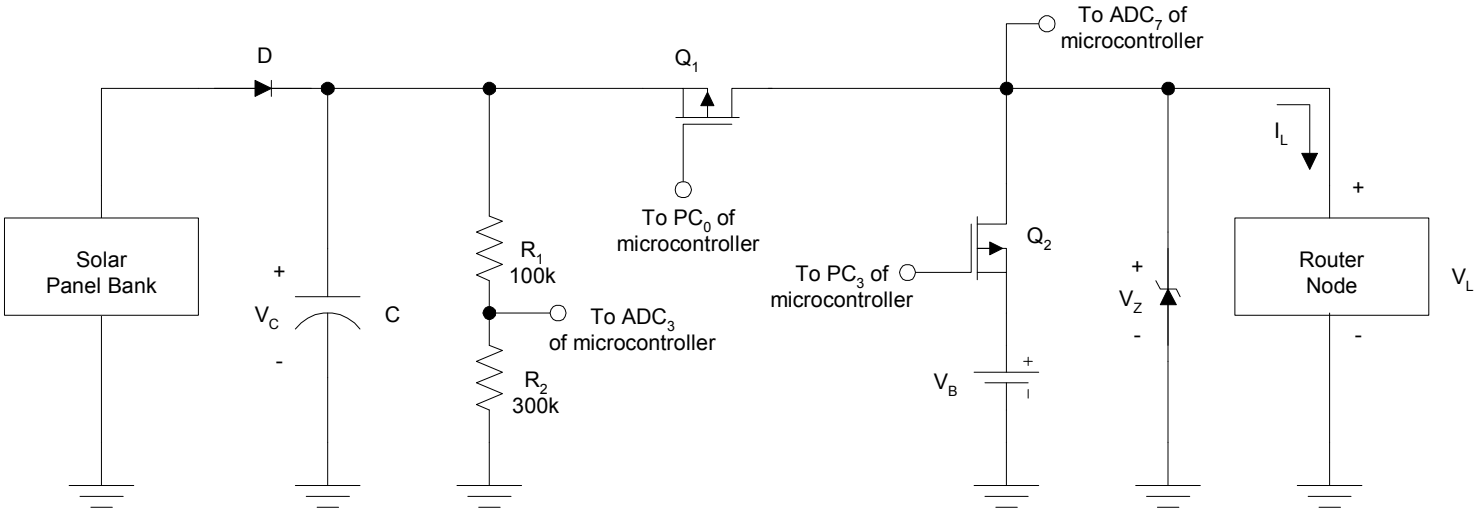

Figure 8. Solar energy harvesting circuit with battery back-up.

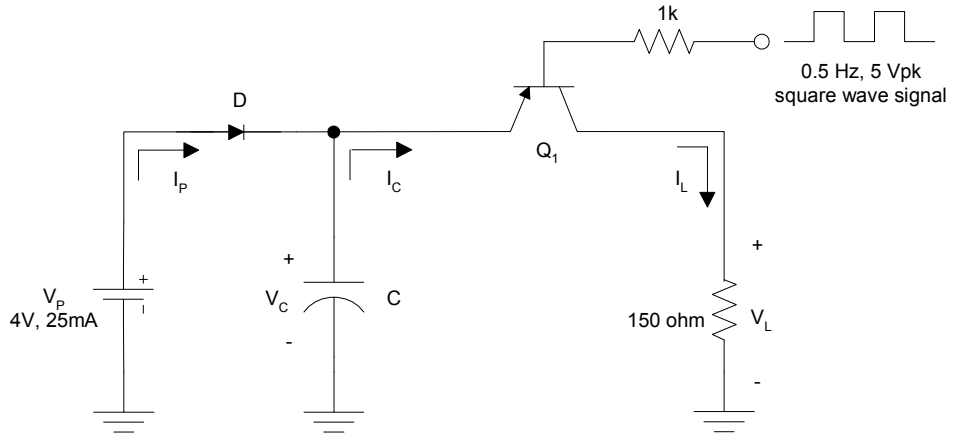

Figure 9. Solar cell simulation test circuit.

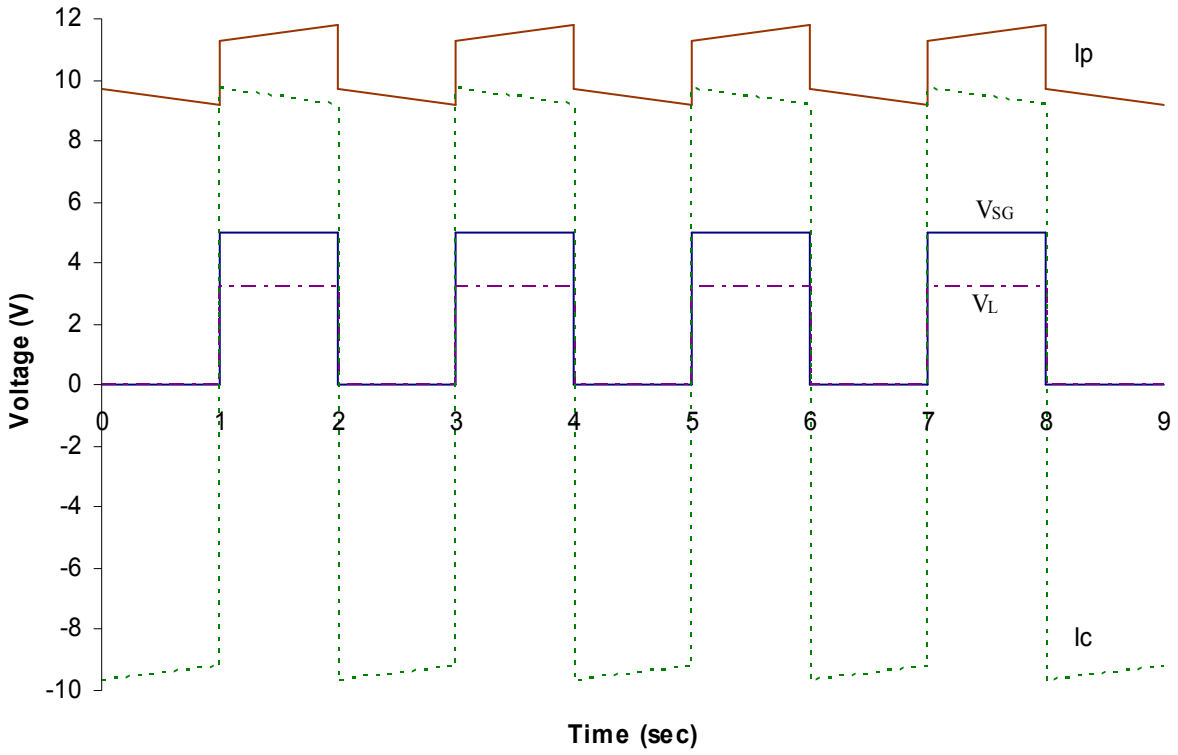

Figure 10. Steady state solar cell simulation test waveforms.

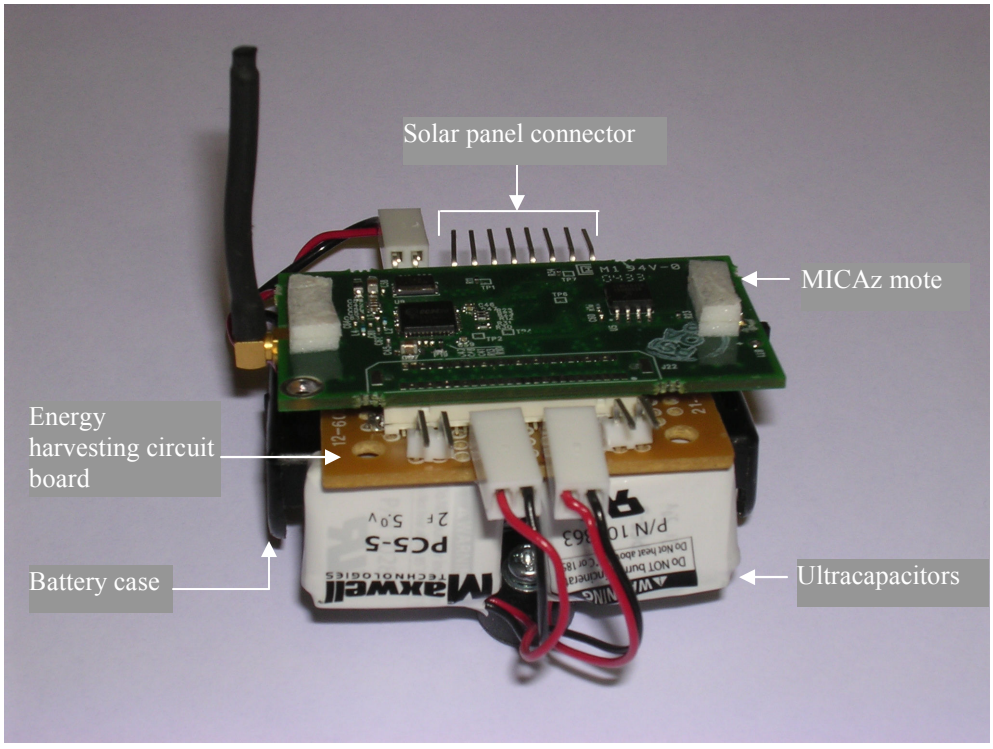

Figure 11. Crossbow MICAz router node with solar energy harvesting prototype circuit.

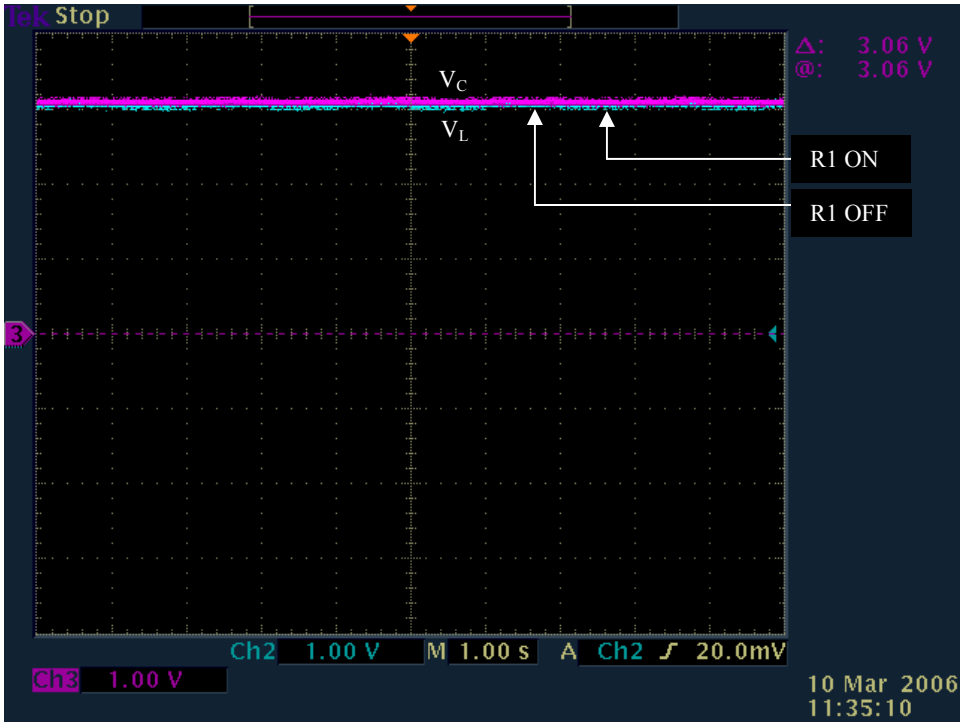

Figure 12. Router node V_L and V_C waveforms.

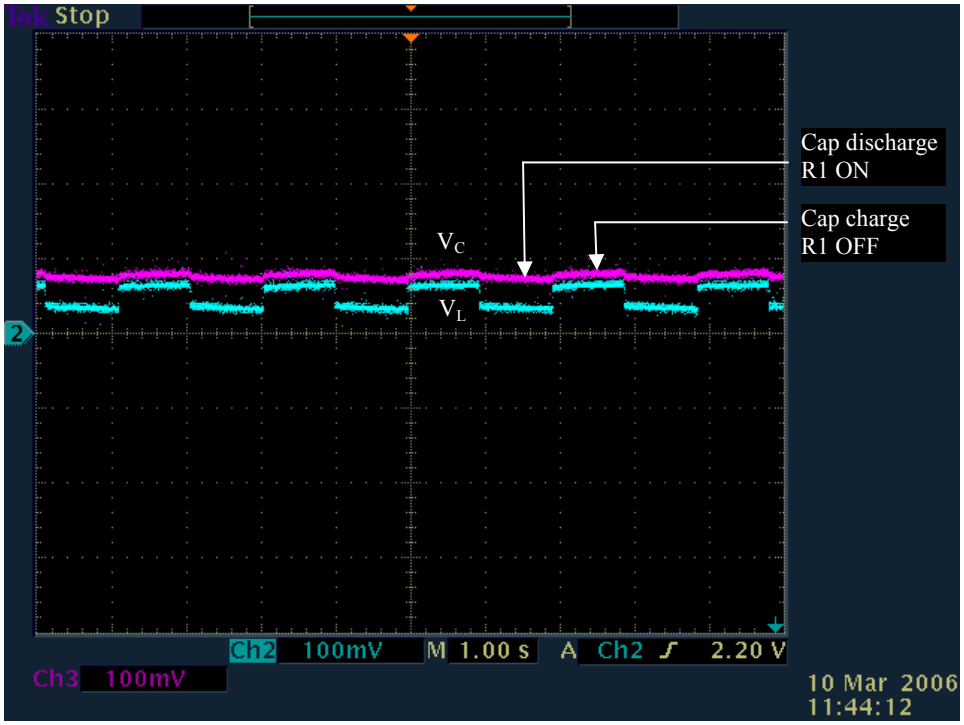

Figure 13. Router node V_L and V_C waveforms indicating ultracapacitor charge and discharge.

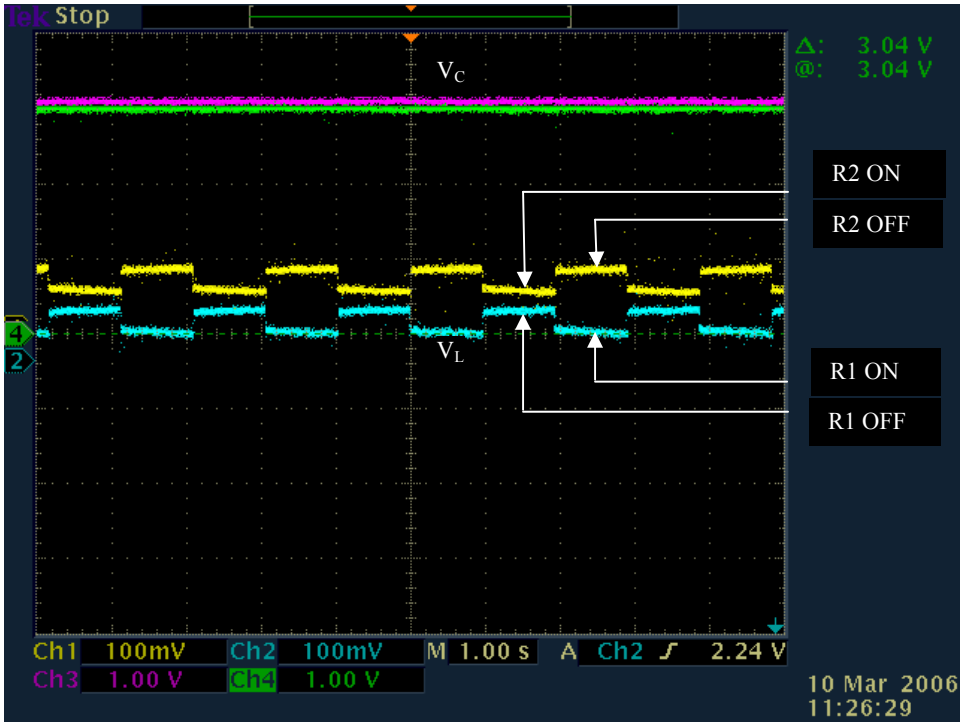

Figure 14. Router pair V_L and V_C waveforms.

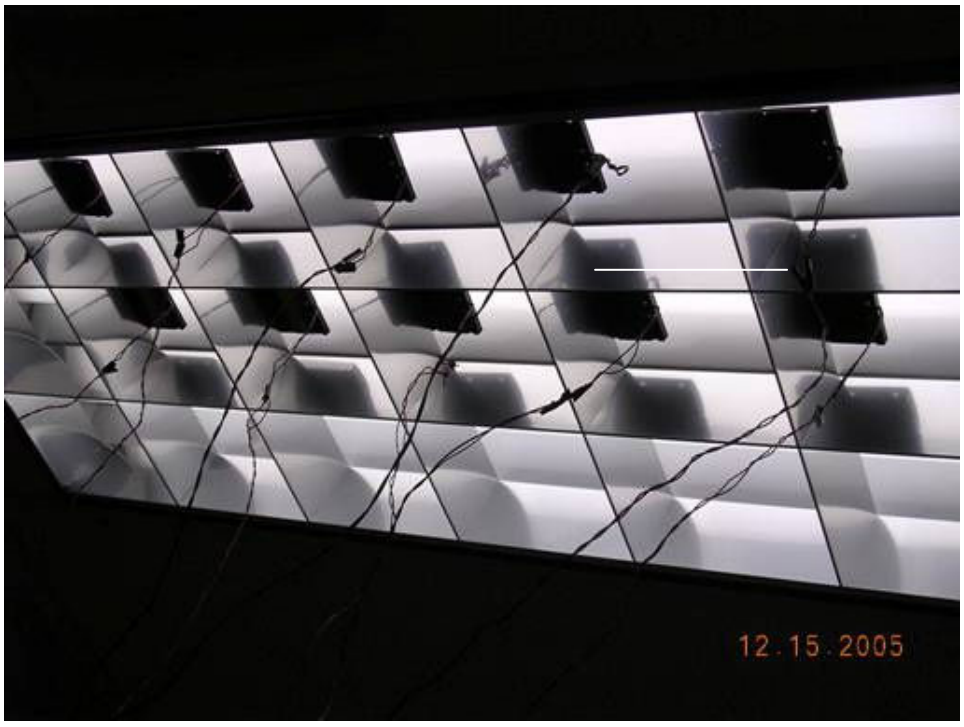

Figure 15. Solar panels set up close to overhead fluorescent lights.

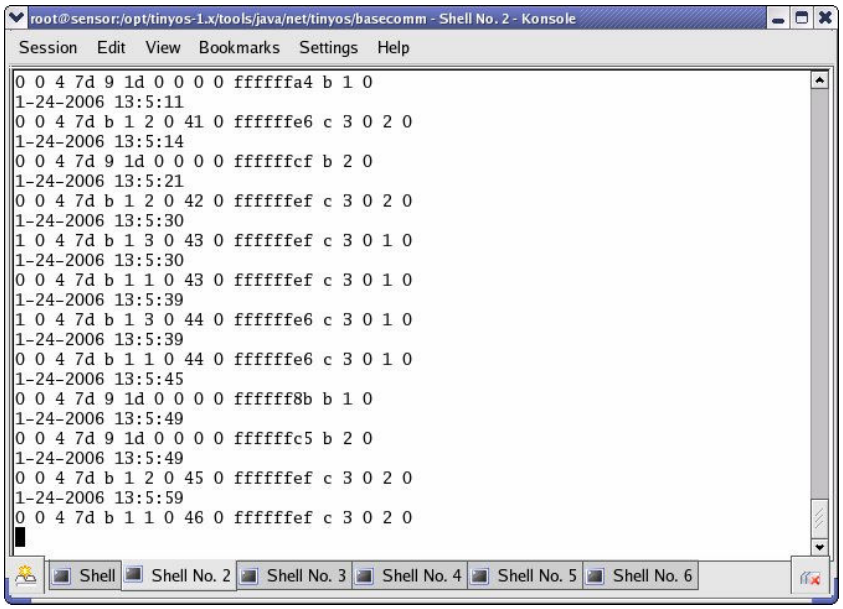

Figure 16. Serial forwarder terminal program

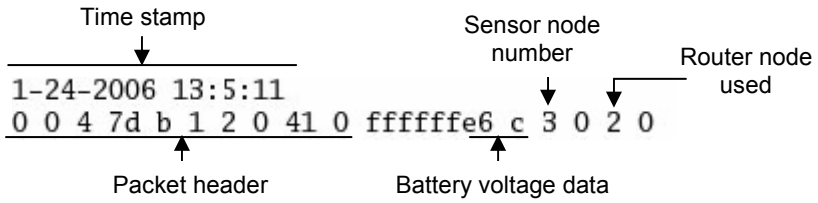

Figure 17. Serial forwarder packet information

Harvesting technology	Power density
Solar cells (outdoors at noon)	15 mW/cm^2
Piezoelectric (shoe inserts)	330 μW/cm^3
Vibration (small microwave oven)	116 μW/cm^3
Thermoelectric (10^{o}C gradient)	40 μW/cm^3
Acoustic noise (100dB)	960 nW/cm^3

Table 1. Power densities of energy harvesting technologies